Modern Homing Missile Guidance Theory and Techniques

Neil F. Palumbo, Ross A. Blauwkamp, and Justin M. Lloyd

Classically derived homing guidance laws, such as proportional navigation, can be highly effective when the homing missile has significantly more maneuver capability than the threat. As threats become more capable, however, higher performance is required from the missile guidance law to achieve intercept. To address this challenge, most modern guidance laws are derived using linear-quadratic optimal control theory to obtain analytic feedback solutions. Generally, optimal control strategies use a cost function to explicitly optimize the missile performance criteria. In addition, it is typical for these guidance laws to employ more sophisticated models of the target and missile maneuver capability in an effort to improve overall performance. In this article, we will present a review of optimal control theory and derive a number of optimal guidance laws of increasing complexity. We also will explore the advantages that such guidance laws have over proportional navigation when engaging more stressing threats

INTRODUCTION

Classical guidance laws, with proportional navigation (PN) being the most prominent example, had proven to be effective homing guidance strategies up through the 1960s and early 1970s. By the mid-1970s, however, the predicted capability of future airborne threats (highly maneuverable aircraft, supersonic cruise missiles, tactical and strategic ballistic missile reentry vehicles, etc.) indicated that PN-guided weapons might be ineffective against them. However, by that time, the application of optimal control theory to missile guidance problems had sufficiently matured, offering new and potentially promising alternative guidance law designs.[1–3] Around this time, the computer power required to mechanize such advanced algorithms also was sufficient to make their application practical.

Most modern guidance laws are derived using linear-quadratic (LQ) optimal control theory to obtain analytic feedback solutions.[1,4,5] Many of the modern

formulations take target maneuver into account to deal with highly maneuvering target scenarios (particularly true for terminal homing guidance). The availability of target acceleration information for the guidance law varies, depending on targeting sensor capability and type and the specific guidance law formulation. Typically, there also is an explicit assumption made about the missile airframe/autopilot dynamic response characteristics in the modern formulations. We will show later that PN is an optimal guidance law in the absence of airframe/autopilot lag (and under certain other assumed conditions). To some extent, the feedback nature of the homing guidance law allows the missile to correct for inaccurate predictions of target maneuver and other unmodeled dynamics (see Fig. 1). However, the requirement for better performance continues to push optimal guidance law development, in part by forcing the consideration (inclusion) of more detailed dynamics of the interceptor and its target. It is interesting that most if not all modern guidance laws derived using optimal control theory can be shown to be supersets of PN.

In the following sections, we first provide a cursory review of dynamic optimization techniques with a focus on LQ optimal control theory. Using this as background, we then develop a number of terminal homing guidance laws based on various assumptions, in the order of assumption complexity. In our companion article in this issue, "Guidance Filter Fundamentals," we introduce guidance filtering, with a focus on Kalman guidance filter techniques.

REVIEW OF LQ OPTIMAL CONTROL

Here, we start by considering a general nonlinear dynamics model of the system to be controlled (i.e., the "plant"). This dynamics model can be expressed as

$$\dot{\bar{\mathbf{x}}}(t) = \bar{\mathbf{f}}(\bar{\mathbf{x}}(t), \bar{\mathbf{u}}(t), t) \, . \tag{1}$$

In Eq. 1, $\bar{\mathbf{x}}$ is the n-dimensional state vector of real elements ($\bar{\mathbf{x}} \in \mathbb{R}^n$), $\bar{\mathbf{u}} \in \mathbb{R}^m$ is the control vector, and t represents time (later we will provide more detail as to the structure of the state and control vectors for the homing guidance problem). With this general system, we associate the following scalar performance index:

$$J(\bar{\mathbf{x}}(t_0), \bar{\mathbf{u}}(t_0), t_0) = \phi(\bar{\mathbf{x}}(t_f), t_f) + \int_{t_0}^{t_f} L(\bar{\mathbf{x}}(t), \bar{\mathbf{u}}(t), t)\, dt \, . \tag{2}$$

In this equation, $[t_0, t_f]$ is the time interval of interest. The performance index comprises two parts: (*i*) a scalar algebraic function of the final state and time (final state penalty), $\phi(\bar{\mathbf{x}}(t_f), t_f)$, and (*ii*) a scalar integral function of the state and control (Lagrangian), $\int_{t_0}^{t_f} L(\bar{\mathbf{x}}(t), \bar{\mathbf{u}}(t), t)\, dt$. The choice of $\phi(\bar{\mathbf{x}}(t_f), t_f)$ and $\int_{t_0}^{t_f} L(\bar{\mathbf{x}}(t), \bar{\mathbf{u}}(t), t)\, dt$ (this choice is a significant part of the design problem) will dictate the nature of the optimizing solution. Thus, the performance index is selected to make the plant in Eq. 1 exhibit desired characteristics and behavior (transient response, stability, etc.).

For our purposes, the optimal control problem is to find a control, $\bar{\mathbf{u}}^*(t)$, on the time interval $[t_0, t_f]$ that drives the plant in Eq. 1 along a trajectory, $\bar{\mathbf{x}}^*(t)$, such that the scalar performance index in Eq. 2 is minimized.

It is difficult to find analytic guidance law expressions for such general nonlinear systems. Therefore, we will turn our attention to a subset of optimal control that can yield tractable analytic solutions, known as the LQ optimal control problem.

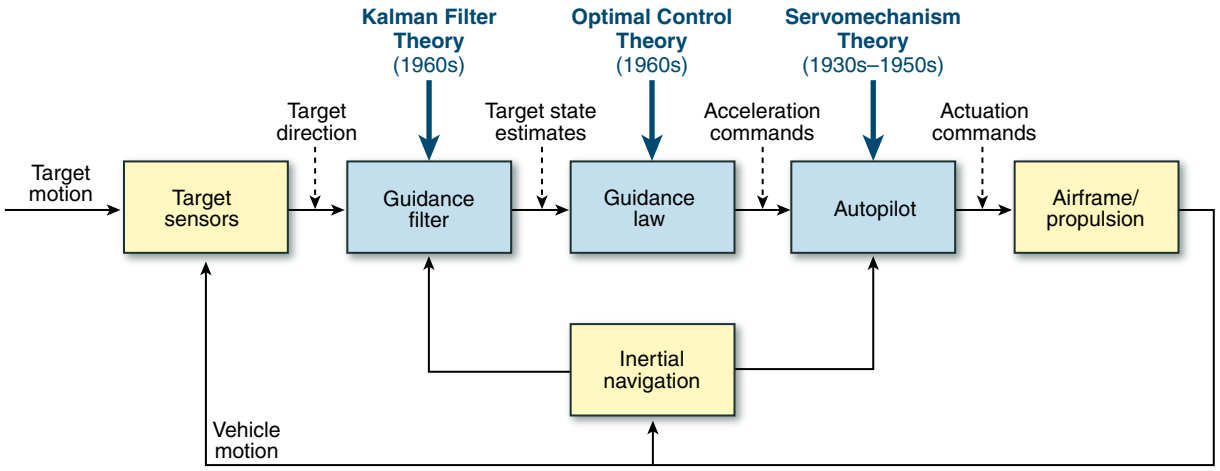

Figure 1. The traditional guidance, navigation, and control topology for a guided missile comprises guidance filter, guidance law, autopilot, and inertial navigation components. Each component may be synthesized by using a variety of techniques, the most popular of which are indicated here in blue text.

The LQ Optimal Control Problem

Here, we assume that the nonlinear model in Eq. 1 can be linearized about an equilibrium point $(\bar{\mathbf{x}}_0, \bar{\mathbf{u}}_0)$ and represented by the time-varying linear dynamic system described in Eq. 3[1,4]:

$$\dot{\bar{\mathbf{x}}}(t) = \mathbf{A}(t)\bar{\mathbf{x}}(t) + \mathbf{B}(t)\bar{\mathbf{u}}(t)\,. \tag{3}$$

In this model (as in the nonlinear case), $\bar{\mathbf{x}} \in \mathbb{R}^n$ is the state vector, $\bar{\mathbf{u}} \in \mathbb{R}^m$ is the control vector, and t represents time. Here, however, $\mathbf{A}(t)$ and $\mathbf{B}(t)$ are the time-varying Jacobian matrices

$$(\partial \bar{\mathbf{f}}(\bar{\mathbf{x}}, \bar{\mathbf{u}}, t)/\partial \bar{\mathbf{x}}|_{\substack{\bar{\mathbf{x}}=\bar{\mathbf{x}}_0 \\ \bar{\mathbf{u}}=\bar{\mathbf{u}}_0}} \text{ and } \partial \bar{\mathbf{f}}(\bar{\mathbf{x}}, \bar{\mathbf{u}}, t)/\partial \bar{\mathbf{u}}|_{\substack{\bar{\mathbf{x}}=\bar{\mathbf{x}}_0 \\ \bar{\mathbf{u}}=\bar{\mathbf{u}}_0}}, \text{respectively})$$

of appropriate dimension.

Using the "shorthand" notation $\|\bar{\mathbf{z}}(t)\|_{\mathbf{S}}^2 \triangleq \bar{\mathbf{z}}^T(t)\mathbf{S}\bar{\mathbf{z}}(t)$, we next define the quadratic performance index (a special case of the performance index shown in Eq. 2) shown in Eq. 4:

$$J(\bar{\mathbf{x}}(t_0), \bar{\mathbf{u}}(t_0), t_0) = \tfrac{1}{2}\|\bar{\mathbf{x}}(t_f)\|_{\mathbf{Q}_f}^2 + \tfrac{1}{2}\int_{t_0}^{t_f}\left[\|\bar{\mathbf{x}}(t)\|_{\mathbf{Q}(t)}^2 + \|\bar{\mathbf{u}}(t)\|_{\mathbf{R}(t)}^2\right]dt\,. \tag{4}$$

In Eq. 4, the following assumptions are made: the terminal penalty weighting matrix, $\mathbf{Q}_f$, is positive semi-definite (the eigenvalues of $\mathbf{Q}_f$ are ≥ 0, expressed as $\mathbf{Q}_f \geq 0$); the state penalty weighting matrix, $\mathbf{Q}(t)$, is positive semi-definite ($\mathbf{Q}(t) \geq 0$); and the control penalty matrix, $\mathbf{R}(t)$, is positive definite ($\mathbf{R}(t) > 0$). Thus, the LQ optimal control problem is to find a control, $\bar{\mathbf{u}}^*(t)$, such that the quadratic cost in Eq. 4 is minimized subject to the constraint imposed by the linear dynamic system in Eq. 3.

To solve this continuous-time optimal control problem, one can use Lagrange multipliers, $\bar{\boldsymbol{\lambda}}(t)$, to adjoin the (dynamic) constraints (Eq. 3) to the performance index (Eq. 4).[1,5] Consequently, an augmented cost function can be written as

$$J' = \tfrac{1}{2}\|\bar{\mathbf{x}}(t_f)\|_{\mathbf{Q}_f}^2 + \int_{t_0}^{t_f}\left[\begin{array}{l}\tfrac{1}{2}\left(\|\bar{\mathbf{x}}(t)\|_{\mathbf{Q}(t)}^2 + \|\bar{\mathbf{u}}(t)\|_{\mathbf{R}(t)}^2\right) \\ + \bar{\boldsymbol{\lambda}}^T(t)\left(\mathbf{A}(t)\bar{\mathbf{x}}(t)\right. \\ \left. + \mathbf{B}(t)\bar{\mathbf{u}}(t) - \dot{\bar{\mathbf{x}}}(t)\right)\end{array}\right]dt\,. \tag{5}$$

Referring to Eq. 5, we define the Hamiltonian function H as shown:

$$H(\bar{\mathbf{x}}(t), \bar{\mathbf{u}}(t), t) = \tfrac{1}{2}\|\bar{\mathbf{x}}(t)\|_{\mathbf{Q}(t)}^2 + \tfrac{1}{2}\|\bar{\mathbf{u}}(t)\|_{\mathbf{R}(t)}^2 + \bar{\boldsymbol{\lambda}}^T(t)\left(\mathbf{A}(t)\bar{\mathbf{x}}(t) + \mathbf{B}(t)\bar{\mathbf{u}}(t)\right). \tag{6}$$

Then, from the calculus of variations, four necessary conditions for optimality must be satisfied[5] to solve our problem: state, costate, boundary, and stationarity conditions must all hold. These four conditions are listed in Table 1.

From Table 1 (and based on our previous description of the dimension of the plant state vector), it can be seen that there is a system of $2n$ dynamic equations that must be solved; n equations must be solved forward in time over $[t_0, t_f]$ (state equations), and n equations must be solved backward in time over $[t_f, t_0]$ (costate equations). We further note that the equations are coupled. Applying the stationarity condition to Eqs. 3–6 yields the following result for the control:

$$\bar{\mathbf{u}}(t) = -\mathbf{R}^{-1}(t)\mathbf{B}^T(t)\bar{\boldsymbol{\lambda}}(t)\,. \tag{7}$$

Using Eq. 7 in the state and costate necessary conditions, and taking into account the boundary condition, leads to the following two-point boundary value problem:

$$\begin{bmatrix}\dot{\bar{\mathbf{x}}}(t) \\ \dot{\bar{\boldsymbol{\lambda}}}(t)\end{bmatrix} = \begin{bmatrix}\mathbf{A}(t) & -\mathbf{B}(t)\mathbf{R}^{-1}\mathbf{B}^T \\ -\mathbf{Q}(t) & -\mathbf{A}^T(t)\end{bmatrix}\begin{bmatrix}\bar{\mathbf{x}}(t) \\ \bar{\boldsymbol{\lambda}}(t)\end{bmatrix}, \quad \left\{\begin{array}{l}\bar{\mathbf{x}}(t_0)\text{given} \\ \bar{\boldsymbol{\lambda}}(t_f) = \mathbf{Q}_f\bar{\mathbf{x}}(t_f)\end{array}\right\}. \tag{8}$$

Here, we are concerned with solution methods that can yield analytic (closed-form) solutions rather than iterative numerical or gain scheduling techniques. We note, however, that the sparseness/structure of the constituent plant and cost matrices—e.g., $\mathbf{A}(t)$, $\mathbf{B}(t)$, $\mathbf{Q}(t)$, and $\mathbf{R}(t)$—will dictate the ease by which this can be accomplished. Qualitatively speaking, the level of difficulty involved in obtaining analytic solutions is related primarily to the complexity of state equation coupling into the costate equations, most notably by the structure of $\mathbf{Q}(t)$ and, to a lesser extent, by the structure of $\mathbf{A}(t)$. As we will see later, however, this fact does not negate our ability to derive effective guidance laws.

Given a suitable system structure in Eqs. 7 and 8 (as discussed above), one conceptually straightforward way to solve this problem is to directly integrate the costate equations backward in time from t_f to $t \geq t_0$ using the terminal costate conditions and then integrate the state

Table 1. Necessary conditions for optimality.

Condition	Expression
State Equation	$\partial H(\bar{\mathbf{x}}(t), \bar{\mathbf{u}}(t), t)/\partial \bar{\boldsymbol{\lambda}}(t) = \dot{\mathbf{x}}(t)$, for $t \geq t_0$
Costate Equation	$\partial H(\bar{\mathbf{x}}(t), \bar{\mathbf{u}}(t), t)/\partial \bar{\mathbf{x}}(t) = -\dot{\bar{\boldsymbol{\lambda}}}(t)$, for $t \leq t_f$
Stationarity	$\partial H(\bar{\mathbf{x}}(t), \bar{\mathbf{u}}(t), t)/\partial \bar{\mathbf{u}}(t) = 0$, for $t \geq t_0$
Boundary	$\partial \phi(\bar{\mathbf{x}}(t_f), t_f)/\partial \bar{\mathbf{x}}(t_f) = \bar{\boldsymbol{\lambda}}(t_f)$, $\bar{\mathbf{x}}(t_0)$ given

equations forward in time using the costate solutions and initial conditions on the states. This process can be done by hand or by using any available symbolic solution software (Maple, Mathematica, etc.). Another way to solve the two-point boundary value problem specified in Eq. 8 employs the sweep method.[1] This technique assumes that the state $\bar{\mathbf{x}}(t)$ and costate $\bar{\boldsymbol{\lambda}}(t)$ satisfy the linear relation shown below over the interval $t \in [t_0, t_f]$ and given an (as yet) unknown matrix function $\mathbf{P}_c(t)$:

$$\bar{\boldsymbol{\lambda}}(t) = \mathbf{P}_c(t)\bar{\mathbf{x}}(t). \tag{9}$$

Using the assumed relation in Eq. 9, the control in Eq. 7 can be written as

$$\bar{\mathbf{u}}(t) = -\mathbf{R}^{-1}(t)\mathbf{B}^T(t)\mathbf{P}_c(t)\bar{\mathbf{x}}(t). \tag{10}$$

To find $\mathbf{P}_c(t)$ such that the control (Eq. 10) is completely defined, we differentiate Eq. 9 and make use of the dynamic equations in Eq. 8. Doing so leads to a requirement to solve the following matrix Riccati differential equation:

$$\begin{aligned} -\dot{\mathbf{P}}_c(t) &= \mathbf{P}_c(t)\mathbf{A}(t) + \mathbf{A}^T(t)\mathbf{P}_c(t) \\ &\quad - \mathbf{P}_c(t)\mathbf{B}(t)\mathbf{R}^{-1}(t)\mathbf{B}^T(t)\mathbf{P}_c(t) \\ &\quad + \mathbf{Q}(t),\ \mathbf{P}_c(t_f) = \mathbf{Q}_f. \end{aligned} \tag{11}$$

The optimal control is determined by first solving the matrix Riccati differential equation backward in time from t_f to t and then using this solution in Eq. 10. There are many ways to solve this equation. For completeness, we present a matrix exponential method of solution.

Solving the Matrix Riccati Differential Equation via Matrix Exponential Method

We first want to rewrite Eq. 11 in terms of the time-to-go variable defined as $t_{go} \triangleq t_f - t$. We use the fact that $dt_{go}/dt = -1$ (for fixed t_f) to express Eq. 11 in terms of t_{go} as shown (note that plant matrices must be time-independent for this technique):

$$\begin{aligned} \dot{\mathbf{P}}_c(t_{go}) &= \mathbf{P}_c(t_{go})\mathbf{A} + \mathbf{A}^T\mathbf{P}_c(t_{go}) \\ &\quad - \mathbf{P}_c(t_{go})\mathbf{B}\mathbf{R}^{-1}\mathbf{B}^T\mathbf{P}_c(t) + \mathbf{Q}, \\ \mathbf{P}_c(t_{go} = 0) &= \mathbf{Q}_f. \end{aligned} \tag{12}$$

Clearly, this matrix differential equation is quadratic in $\mathbf{P}_c(t_{go})$ and is of dimension n. Note, however, that if we assume that $\mathbf{P}_c(t_{go})$ takes the form $\mathbf{P}_c(t_{go}) = \mathbf{Y}(t_{go})\mathbf{W}^{-1}(t_{go})$, then its solution may (instead) be found by solving the homogeneous linear matrix differential equation of dimension $2n$ shown in Eq. 13:

$$\frac{d}{dt_{go}}\begin{bmatrix}\mathbf{W}(t_{go}) \\ \hline \mathbf{Y}(t_{go})\end{bmatrix} = \left[\begin{array}{c|c} -\mathbf{A} & \mathbf{B}\mathbf{R}^{-1}\mathbf{B}^T \\ \hline \mathbf{Q} & \mathbf{A}^T \end{array}\right]\begin{bmatrix}\mathbf{W}(t_{go}) \\ \hline \mathbf{Y}(t_{go})\end{bmatrix}. \tag{13}$$

From linear system theory, we know that the solution to Eq. 13 can be expressed by the following matrix exponential:

$$\begin{bmatrix}\mathbf{W}(t_{go}) \\ \hline \mathbf{Y}(t_{go})\end{bmatrix} = \exp(\boldsymbol{\Psi} t_{go})\begin{bmatrix}\mathbf{W}(t_{go} = 0) \\ \hline \mathbf{Y}(t_{go} = 0)\end{bmatrix}, \qquad \boldsymbol{\Psi} \triangleq \left[\begin{array}{c|c} -\mathbf{A} & \mathbf{B}\mathbf{R}^{-1}\mathbf{B}^T \\ \hline \mathbf{Q} & \mathbf{A}^T \end{array}\right]. \tag{14}$$

In Eq. 14, $\boldsymbol{\Psi}$ is the Hamiltonian matrix. With regard to ease of determining analytic solutions, in an analogous way to our previous discussion, the complexity of the system structure (and the system order) will dictate how difficult it may be to obtain an analytic solution to the matrix exponential $\exp(\boldsymbol{\Psi} t_{go})$. Once an analytic solution is found, the exponential matrix solution is partitioned as shown:

$$\exp(\boldsymbol{\Psi} t_{go}) \equiv \left[\begin{array}{c|c} \boldsymbol{\psi}_{11}(t_{go}) & \boldsymbol{\psi}_{12}(t_{go}) \\ \hline \boldsymbol{\psi}_{21}(t_{go}) & \boldsymbol{\psi}_{22}(t_{go}) \end{array}\right]. \tag{15}$$

Using Eq. 15, the relation $\mathbf{P}_c(t_{go}) = \mathbf{Y}(t_{go})\mathbf{W}^{-1}(t_{go})$, $\mathbf{Y}(0) \equiv \mathbf{Q}_f$, $\mathbf{W}(0) = \mathbf{I}$, and the initial condition from Eq. 12 ($\mathbf{P}_c(t_{go} = 0) = \mathbf{Q}_f$), the solution to the matrix Riccati differential equation $\mathbf{P}_c(t_{go})$ can be expressed as

$$\begin{aligned} \mathbf{P}_c(t_{go}) &= [\boldsymbol{\psi}_{21}(t_{go}) + \boldsymbol{\psi}_{22}(t_{go})\mathbf{Q}_f] \\ &\quad [\boldsymbol{\psi}_{11}(t_{go}) + \boldsymbol{\psi}_{12}(t_{go})\mathbf{Q}_f]^{-1}. \end{aligned} \tag{16}$$

From Eq. 16, it becomes clear that the existence of $\mathbf{P}_c(t_{go})$ is equivalent to having a nonsingular $\boldsymbol{\psi}_{11}(t_{go}) + \boldsymbol{\psi}_{12}(t_{go})\mathbf{Q}_f$. (We do not explore this important issue here, but the interested reader is referred to Refs. 1 and 4–11 for further treatment of the subject.) Using Eq. 16 in Eq. 10, the optimal control then is fully specified. Hand calculations (for systems of low order) or symbolic solution software can be employed to mechanize this technique.

THE PLANAR INTERCEPT PROBLEM

In general, the guidance process takes place in three-dimensional space. However, such analysis can be complex and is beyond the scope of this article. Thus, here we will consider the formulation of the planar intercept (pursuit-evasion) problem that we will use, subsequently, in the derivation of a number of different modern guidance laws. This approach is not overly restrictive or unrealistic in that many (if not most) guidance law implementations, including modern ones, use the same approach, i.e., planar guidance laws are devised and implemented in each of the maneuver planes. Figure 2 illustrates the planar (two-dimensional) engagement geometry and defines the angular and Cartesian quantities depicted therein. In Fig. 2, the x axis represents

γ_M = Missile flight path angle
γ_T = Target flight path angle
λ = LOS angle
$\bar{\mathbf{r}}_M$ = Missile inertial position vector
$\bar{\mathbf{r}}_T$ = Target inertial position vector
$\bar{\mathbf{v}}_M$ = Missile velocity vector
$\bar{\mathbf{v}}_T$ = Target velocity vector
$\bar{\mathbf{a}}_M$ = Missile acceleration, normal to LOS
$\bar{\mathbf{a}}_T$ = Target acceleration, normal to V_T
L = Lead angle
r_x = Relative position x ($r_{Tx} - r_{Mx}$)
r_y = Relative position y ($r_{Ty} - r_{My}$)
R = Range to target

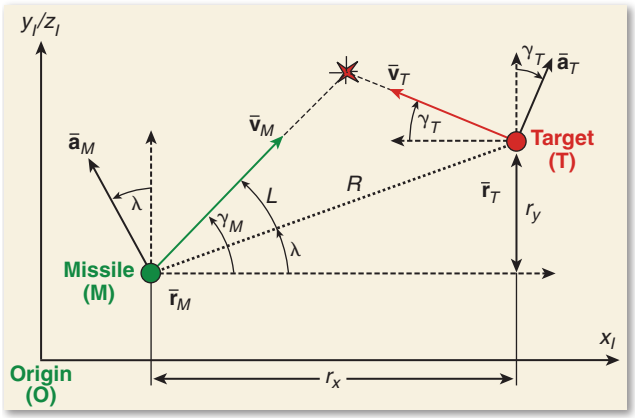

Figure 2. Planar engagement geometry. The planar intercept problem is illustrated along with most of the angular and Cartesian quantities necessary to derive modern guidance laws. The *x* axis represents downrange while the *y*/*z* axis can represent either crossrange or altitude. A flat-Earth model is assumed with an inertial coordinate system that is fixed to the surface of the Earth. The positions of the missile (M) and target (T) are shown with respect to the origin (O) of the coordinate system. Differentiation of the target–missile relative position vector yields relative velocity; double differentiation yields relative acceleration.

downrange, for example, while the *y*/*z* axis can represent either crossrange or altitude, respectively (we will use *y* below). For simplicity, we assume a flat-Earth model with an inertial coordinate system that is fixed to the surface of the Earth. Furthermore, we will assume that the missile and target speeds, $\|\bar{\mathbf{v}}_M\|$ and $\|\bar{\mathbf{v}}_T\|$, respectively, are constant.

In Fig. 2, the positions of the missile (pursuer) *M* and target (evader) *T* are shown with respect to the origin (*O*) of the coordinate system, $\bar{\mathbf{r}}_M$ and $\bar{\mathbf{r}}_T$, respectively. Thus, the relative position vector [or line-of-sight (LOS) vector, as it was previously defined] is given by $\bar{\mathbf{r}} = \bar{\mathbf{r}}_T - \bar{\mathbf{r}}_M$, and the relative velocity vector is given by $\dot{\bar{\mathbf{r}}} \triangleq \bar{\mathbf{v}} = \bar{\mathbf{v}}_T - \bar{\mathbf{v}}_M$. From Fig. 2, note that an intercept condition is satisfied if $\hat{y} = 0$ and $V_c > 0$ (i.e., a collision triangle condition). As illustrated, for this condition to be satisfied, the missile velocity vector must lead the LOS by the lead angle *L*. Determining the lead angle necessary to establish a collision triangle is, implicitly, a key purpose of the guidance law. How this is done is a factor of many things, including what measurements are available to the guidance system and what assumptions were made during formulation of the guidance law (e.g., a non-maneuvering target was assumed).

The homing kinematics can be expressed in various ways. Here, we concentrate on Cartesian forms of expression. From a previous section, the target-to-missile range was defined as $R = \|\bar{\mathbf{r}}\|$, and target–missile closing velocity was defined as $V_c \triangleq -\dot{R} \equiv -\bar{\mathbf{v}} \cdot \bar{\mathbf{1}}_{\mathbf{r}}$, where the LOS unit vector is $\bar{\mathbf{1}}_{\mathbf{r}} = \bar{\mathbf{r}}/R$. Thus, referring to Fig. 2, expressions for target–missile relative position, relative velocity, and relative acceleration are given below, where we have defined the quantities $v_M \triangleq \|\bar{\mathbf{v}}_M\|$, $a_M \triangleq \|\bar{\mathbf{a}}_M\|$, $v_T \triangleq \|\bar{\mathbf{v}}_T\|$, and $a_T \triangleq \|\bar{\mathbf{a}}_T\|$.

$$
\begin{aligned}
\bar{\mathbf{r}} &= r_x \bar{\mathbf{1}}_x + r_y \bar{\mathbf{1}}_y = [R\cos(\lambda)]\bar{\mathbf{1}}_x + [R\sin(\lambda)]\bar{\mathbf{1}}_y \\
\bar{\mathbf{v}} &= v_x \bar{\mathbf{1}}_x + v_y \bar{\mathbf{1}}_y = [\{-v_T\cos(\gamma_T) - v_M\cos(L+\lambda)\}]\bar{\mathbf{1}}_x \\
&\quad + [\{v_T\sin(\gamma_T) - v_M\sin(L+\lambda)\}]\bar{\mathbf{1}}_y \qquad (17) \\
\bar{\mathbf{a}} &= a_x \bar{\mathbf{1}}_x + a_y \bar{\mathbf{1}}_y = [\{a_T\sin(\gamma_T) + a_M\sin(\lambda)\}]\bar{\mathbf{1}}_x \\
&\quad + [\{a_T\cos(\gamma_T) - a_M\cos(\lambda)\}]\bar{\mathbf{1}}_y
\end{aligned}
$$

Referring again to Fig. 2, we note that if the closing velocity is positive ($V_c > 0$), then we only need to actively control the kinematics in the *y*/*z* coordinate to achieve an intercept. That is, if $V_c > 0$ and the missile actively reduces and holds r_y to zero by appropriately accelerating normal to the LOS, then r_x will continue to decrease until collision occurs. We will assume this condition holds and disregard the *x* components in the following analysis.

The homing kinematics shown in Eqs. 17 are clearly nonlinear. In order to develop guidance laws using linear optimal control theory, the equations of motion must be linear. Referring to the expression for relative position in Eqs. 17, note that for λ very small, the *y*-axis component of relative position is approximately given by $r_y \approx R\lambda$. Moreover, for very small γ_T and λ (e.g., near-collision course conditions), the *y*-axis component of relative acceleration is approximately given by $a_y \approx a_T - a_M$. Hence, given the near-collision course conditions, we can draw the linearized block diagram of the engagement kinematics as shown in Fig. 3. Correspondingly, we will express the kinematic equations

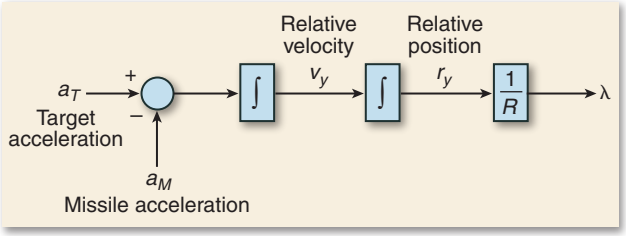

Figure 3. Linear engagement kinematics. Planar linear homing loop kinematics are illustrated here. The integral of target–missile relative acceleration yields relative velocity; double integration yields relative position. The LOS angle, λ, is obtained by dividing relative position by target–missile range.

of motion in state-space form. To this end, we define the state vector $\bar{\mathbf{x}} \triangleq [x_1 \;\; x_2]^T$, the control u, the plant disturbance w, and the pseudo-measurement y where $x_1 \triangleq r_y$, $x_2 \triangleq v_y$, $u \triangleq a_M$, $w \triangleq a_T$ (any residual target acceleration is treated as a disturbance), and $y \triangleq R\lambda$ (the linearized Cartesian pseudo-measurement is composed of range times the LOS angle). Given these definitions, the kinematic equations of motion in state-space form are written as

$$\dot{\bar{\mathbf{x}}}(t) = \mathbf{A}\bar{\mathbf{x}}(t) + \mathbf{B}u(t) + \mathbf{D}w(t), \;\; \bar{\mathbf{x}}_0 = \bar{\mathbf{x}}(0)$$
$$y(t) = \mathbf{C}\bar{\mathbf{x}}(t) \qquad (18)$$
$$\mathbf{A} = \begin{bmatrix} 0 & 1 \\ 0 & 0 \end{bmatrix}, \;\; \mathbf{B} = \begin{bmatrix} 0 \\ -1 \end{bmatrix}, \;\; \mathbf{C} = [1 \;\; 0], \;\; \mathbf{D} = \begin{bmatrix} 0 \\ 1 \end{bmatrix}.$$

These equations will form the basis for developing a number of terminal homing guidance laws in the following subsections. In some cases, the equations are modified or expanded as needed to reflect additional assumptions or special conditions.

DERIVATION OF PN GUIDANCE LAW VIA LQ OPTIMIZATION

In the previous article in this issue, "Basic Principles of Homing Guidance," a classical development of PN guidance was given based on that found in Ref. 12. In the present article, we will leverage off the discussion of the previous subsection and develop a planar version of the PN guidance law using LQ optimization techniques. To start, we will state the key assumptions used to develop the guidance law:

- We use the linear engagement kinematics model discussed previously and, hence, the state vector is $\bar{\mathbf{x}}(t) = [x_1(t) \;\; x_2(t)]^T$ (the state vector comprises the components of relative position and relative velocity perpendicular to the reference x axis shown in Fig. 2).
- All the states are available for feedback.
- The missile and target speeds, $v_M = \|\bar{\mathbf{v}}_M\|$ and $v_T = \|\bar{\mathbf{v}}_T\|$, respectively, are constant.
- The missile control variable is commanded acceleration normal to the reference x axis ($u = a_c$), which, for very small LOS angles (λ), is approximately perpendicular to the instantaneous LOS.
- The target is assumed to be nonmaneuvering ($a_T = 0$) and, therefore, the linear plant disturbance is given to be $w = 0$.
- The missile responds perfectly (instantaneously) to an acceleration command from the guidance law ($a_M \equiv a_c$).The system pseudo-measurement is relative position $y = x_1$.

With these assumptions in mind, and referring to Eq. 18, the LQ optimization problem is stated as

$$\min_{u(t)} J(\bar{\mathbf{x}}(t_0), \bar{\mathbf{u}}(t_0), t_0) = \tfrac{1}{2}\|\bar{\mathbf{x}}(t_f)\|^2_{\mathbf{Q}_f} + \tfrac{1}{2}\int_{t_0}^{t_f} u^2(t)\,dt$$
$$\text{Subject to: } \dot{\bar{\mathbf{x}}}(t) = \begin{bmatrix} 0 & 1 \\ 0 & 0 \end{bmatrix}\bar{\mathbf{x}}(t) + \begin{bmatrix} 0 \\ -1 \end{bmatrix}u(t), \qquad (19)$$
$$y(t) = [1 \;\; 0]\bar{\mathbf{x}}(t).$$

In words, find a minimum-energy control $u(t)$ on the time interval $[t_0, t_f]$ that minimizes a quadratic function of the final (terminal) relative position and relative velocity and subject to the specified dynamic constraints. In Eq. 19, the terminal performance weighting matrix, $\mathbf{Q}_f$, is yet to be specified. We define the scalar $b > 0$ as the penalty on relative position at time t_f (i.e., final miss distance) and scalar $c \geq 0$ as the penalty on relative velocity at t_f (c specified as a positive nonzero value reflects some desire to control or minimize the terminal lateral relative velocity as is the case for a rendezvous maneuver). Given the penalty variables, $\mathbf{Q}_f$ is the diagonal matrix given in Eq. 20:

$$\mathbf{Q}_f = \begin{bmatrix} b & 0 \\ 0 & c \end{bmatrix}. \qquad (20)$$

The choice of b and c is problem-specific, but for intercept problems we typically let $b \to \infty$, $c = 0$, and for rendezvous problems we have $b \to \infty$, $c \to \infty$.

General Solution for Nonmaneuvering Target

We can solve the design problem posed in Eq. 19 by using the LQ solution method discussed previously. We define $t_{go} \triangleq t_f - t$ and initially assume the scalar variables b and c are finite and nonzero. Using Maple, we symbolically solve Eqs. 15 and 16 to obtain an analytic expression for $\mathbf{P}_c(t)$. We then use $\mathbf{P}_c(t)$ in Eq. 10 to obtain the following general guidance law solution:

$$u_1(t) = \frac{3}{t_{go}^2}\left[\frac{\left(1 + \frac{1}{2}ct_{go}\right)x_1(t) + \left(1 + \frac{1}{3}ct_{go} + \frac{c}{bt_{go}^2}\right)x_2(t)t_{go}}{1 + \frac{3}{bt_{go}^3}(1 + ct_{go}) + \frac{ct_{go}}{4}}\right]. \qquad (21)$$

We emphasize the fact that this general solution is relevant given the assumptions enumerated above, particularly the fact that a nonmaneuvering target and perfect interceptor response to commanded acceleration are assumed.

The structure of the guidance law $u_1(t)$, shown above, can be expressed as

$$u_1(t) = \left[\tilde{N}(\mathbf{Q}_f, t_{go})/t_{go}^2\right]z(\bar{\mathbf{x}}, \mathbf{Q}_f, t_{go}),$$

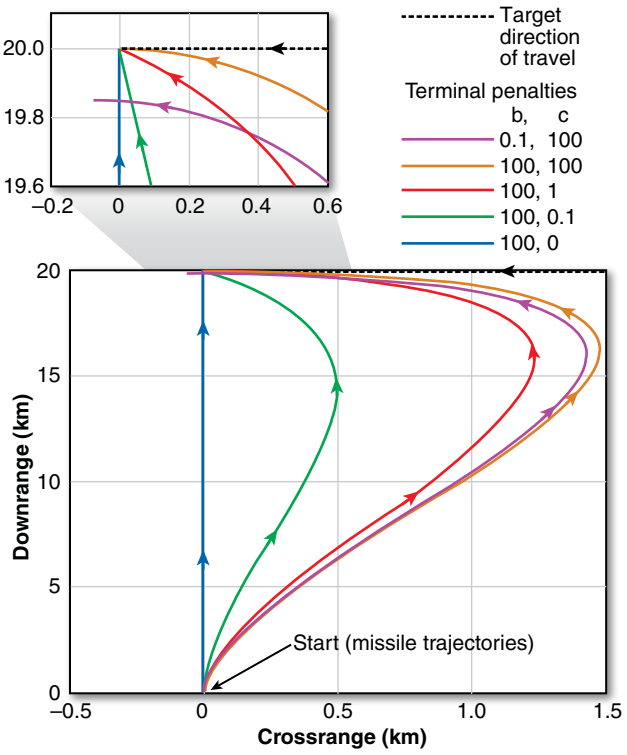

Figure 4. Rendezvous trajectory. A plot of intercept trajectories (in downrange and crossrange) are shown with different terminal penalties for relative position and relative velocity, respectively. The target trajectory is traveling from right to left (shown as the dashed black line) at the top. The target velocity is a constant 500 m/s. The initial missile velocity is 1000 m/s with no heading error. The final time is 20 s. The inset highlights the endgame geometries in each case. Notice that as the terminal penalty on relative velocity is increased, the missile trajectory tends to "bow out" such that the final missile velocity can be aligned with the target velocity. Similarly, as the terminal penalty on relative position increases, the final miss distance is reduced.

where the quantity

$$\tilde{N}(\mathbf{Q}_f, t_{go}) \triangleq 3/\left(1 + \frac{3}{bt_{go}^3}(1 + ct_{go}) + \frac{ct_{go}}{4}\right)$$

is the effective navigation ratio and $z(\bar{\mathbf{x}}, \mathbf{Q}_f, t_{go})$ comprises the remainder of the numerator in Eq. 21. Thus, for this general case, the effective navigation ratio is not a constant value.

It is clear that mechanization of this guidance law requires feedback of the relative position and relative velocity states to compute the control solution. Typically, only the relative position pseudo-measurement is available, formed using measurements of LOS angle and range (assuming a range measurement is available). In our companion article in this issue, "Guidance Filter Fundamentals," we discuss filtering techniques that enable us to estimate any unmeasured but observable states for feedback. From above, we also see that time-to-go (t_{go}) is needed in the guidance law. Later, we also discuss how one can estimate time-to-go for use in the control solution.

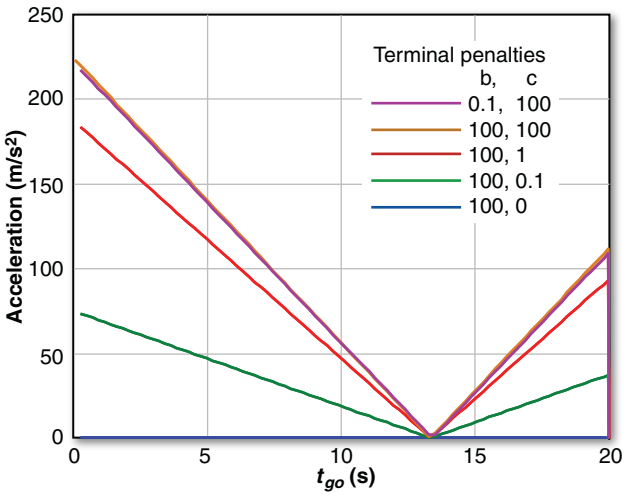

Figure 5. Rendezvous acceleration. A plot of called-for accelerations for intercept trajectories with differing terminal relative position and relative velocity penalties is shown here. The engagement is the same as in Fig 4. As can be seen, substantially more acceleration is required as the penalty on the terminal relative velocity is increased.

Employing Eq. 21 in a simple planar engagement simulation, we can show what effect a terminal relative velocity penalty will have (in combination with a terminal relative position penalty) on the shape of the missile trajectory. In Fig. 4, a missile is on course to intercept a constant-velocity target; it can be seen that the missile trajectory shape changes for different terminal relative position and velocity penalties (i.e., variations in the penalty weights b and c). Note that, in this simple example, there is no assumption that controlled missile acceleration is restricted to the lateral direction. Figure 5 shows the resulting acceleration history for each case. Note that with a nonzero terminal penalty on relative position in combination with no penalty on relative velocity (the blue curve in Fig. 5) the missile does not maneuver at all; this is because the target maneuver assumption implicit in the guidance law derivation (i.e., the target will not maneuver) happens to be correct in this case, and the missile is already on a collision course at the start of the engagement.

Special Case 1: PN Guidance Law

If we assume that $c = 0$ and we evaluate $\lim_{b \to \infty} u_1(t) = u_{PN}(t)$, then Eq. 21 collapses to the well-known Cartesian form of the PN guidance law:

$$u_{PN}(t) = \frac{3}{t_{go}^2}[x_1(t) + x_2(t)t_{go}]. \qquad (22)$$

Leveraging the discussion above for Eq. 21, we can see that the effective navigation ratio in Eq. 21 has now collapsed to become $\tilde{N}|_{PN} = 3$.

In Eq. 22, the quantity in square brackets now represents the miss distance that would result if the missile and target did not maneuver over the time period $[t, t_f]$, which often is referred to as the zero-effort-miss (ZEM). We want to emphasize that the guidance law ZEM is an estimate of future miss that is parameterized on the assumptions upon which the guidance law was derived (linear engagement, constant velocity, non-maneuvering target, etc.). Hence, the PN ZEM (in the y axis, for example) is given by $\mathrm{ZEM}_{PN} = r_y(t) + v_y(t)t_{go}$. Note that the accuracy of the guidance law ZEM estimate is directly related to how well the guidance law will perform in any particular engagement (actual final miss distance, maximum commanded acceleration, amount of fuel used, etc.).

Under the current stated assumptions, we can show that Eq. 22 is equivalent to the traditional LOS rate expression for PN, which was shown in the previous article in this issue, "Basic Principles of Homing Guidance," to be $a_{Mc} = NV_c\dot{\lambda}$. We first differentiate $r_y \approx R\lambda$ to obtain $v_y \approx \dot{R}\lambda + R\dot{\lambda}$. Next, recalling that $\dot{R} = \bar{\mathbf{v}} \bullet \bar{\mathbf{I}}_\mathbf{r} = -V_c$ and noting that we can express range-to-go as $R = V_c t_{go}$, we have the following relationship for LOS rate:

$$\dot{\lambda} = \frac{r_y + v_y t_{go}}{V_c t_{go}^2}. \qquad (23)$$

Examining the traditional LOS rate expression for PN, as well as Eqs. 22 and 23, it can be seen that if we set $N = 3$, then the traditional LOS rate expression for PN and Eq. 22 are equivalent expressions. Hence, the "optimal" PN navigation gain is $N = 3$.

Special Case 2: Rendezvous Guidance Law

For the classic rendezvous problem, we desire to converge on and match the velocity vector of the target at the final time t_f. If we evaluate $\lim_{b,c,\to\infty} u_1(t) = u_{\mathrm{REN}}(t)$, then Eq. 21 collapses to the Cartesian form of the rendezvous (REN) guidance law

$$u_{\mathrm{REN}}(t) = \frac{6}{t_{go}^2}\left[x_1(t) + \tfrac{2}{3}x_2(t)t_{go}\right]. \qquad (24)$$

Example Results

The example in this section is illustrated by Fig. 6, where we demonstrate how PN performance degrades if (*i*) the interceptor response is not ideal (i.e., the actual interceptor response deviates from that assumed in the derivation of PN) and (*ii*) the target performs an unanticipated maneuver some time during the terminal homing portion of the engagement. A planar (downrange and crossrange) Simulink terminal homing simulation was used to examine the PN performance. To avoid layering of complexity in the results, all simulation noise sources (seeker noise, gyro noise, etc.) were turned off for this study. However, a simplified guidance filter still was used in the loop to provide estimates of relative position and velocity to the PN guidance law, thereby having some effect on overall guidance performance. Figure 6a illustrates nominal missile and target trajectories in a plot of downrange versus crossrange. The total terminal homing time is about 3 s. As is evident, at the start of terminal homing, the missile is traveling in from the left (increasing downrange) and the target is traveling in from the right (decreasing downrange). The missile, under PN guidance, is initially on a collision course with the target, and the target is, initially, non-maneuvering. At 2 s time-to-go, the target pulls a hard turn in the increasing crossrange direction.

Recall that PN assumes that the missile acceleration response to guidance commands is perfect or instantaneous (i.e., no-lag), and that the target does not maneuver. Thus, we will examine the sensitivity of PN to these assumptions by simulating a non-ideal missile acceleration response in addition to target maneuver. We will parametrically scale the nominal missile autopilot time constant (100 ms for our nominal case), starting with a scale factor of 1 (the nominal or near-perfect response) up to 5 (a very "sluggish" response of approximately 500 ms) and examine the effect on guidance performance. Figure 6b illustrates the acceleration step response of the interceptor for 100-, 300-, and 500-ms time constants. Figures 6c and 6d present the simulation results for levels of target hard-turn acceleration from 0 to 5 *g*. Figure 6c shows final miss distance versus target hard-turn acceleration level for the three different interceptor time constants. As can be seen, as the missile time response deviates from the ideal case, guidance performance (miss distance) degrades as target maneuver levels increase. Figure 6d illustrates the magnitude of missile total achieved acceleration for variation of target maneuver *g* levels shown and for the three missile time constants considered. As can be seen, when the missile autopilot response time deviates further from that which PN assumes, respectively higher acceleration is required from the missile; this is further exacerbated by higher target *g* levels.

EXTENSIONS TO PN: OTHER OPTIMAL HOMING GUIDANCE LAWS

In Eq. 21, a general guidance law that is based on some specific assumptions regarding the (linearized)

engagement kinematics, target maneuver (actually, a lack of it), and interceptor response characteristics (the perfect response to an acceleration command) is shown. We also showed that the general optimal guidance law derived there collapses to the well-known PN guidance law if we assign cost function components as $c = 0$ and $b \to \infty$ (see Eqs. 19 and 20). For completeness' sake, here we will derive a number of related optimal guidance laws under differing assumptions regarding target maneuver and interceptor response models. For certain scenarios, these assumptions can have a significant impact on guidance law performance. For example, in *Example Results*, it was observed that, during the endgame, PN (which is derived assuming no target maneuver) can call for significant acceleration from the interceptor when pitted against a target pulling a hard-turn maneuver. Hence, one can develop a guidance law that specifically takes target acceleration into account. Of course, mechanization of such a guidance law will be more complex and will require the feedback of additional information (e.g., target maneuver). In addition, if the derivation assumptions become too specific, the resulting guidance law may work well if those assumptions actually hold, but performance might rapidly degrade as reality deviates from the assumptions.

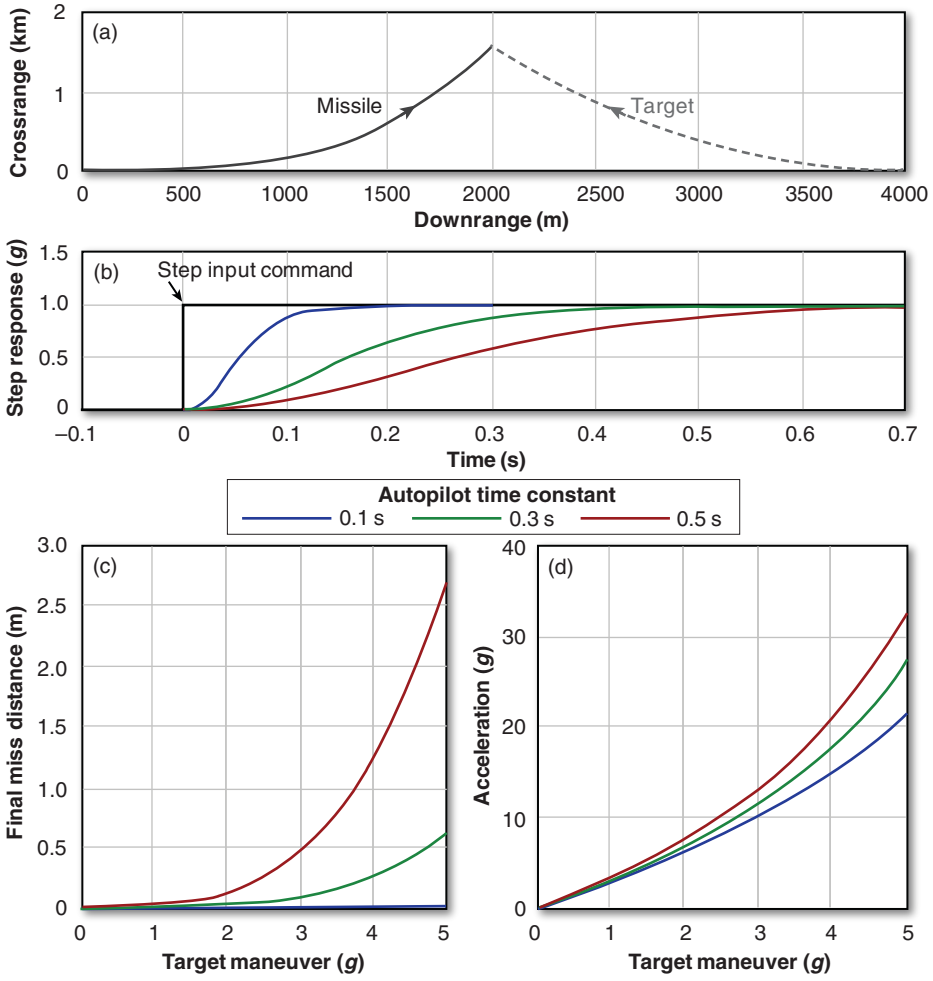

Figure 6. PN performance versus time constant. (a) A planar missile–target engagement with a plot of downrange versus crossrange. The total terminal homing time is approximately 3 s. At the start of terminal homing, the missile is traveling in from the left (increasing downrange) and the target is traveling in from the right (decreasing downrange). (b) The acceleration step response of the missile interceptor for 100-, 300-, and 500-ms time constants. (c and d) Simulation results for a PN-guided missile versus varying levels of target hard-turn acceleration from 0 to 5 *g*. (c) Final miss distance versus target hard-turn acceleration level for the three different interceptor time constants. The graph illustrates the fact that, for non-ideal interceptor response, PN-homing guidance performance degrades with increasing target maneuver levels. This degradation worsens as the autopilot response becomes more sluggish. Notice that as the autopilot response approaches the ideal case (blue curve), the miss distance becomes nearly insensitive to target maneuver. For an ideal autopilot response, PN-homing would result in acceleration requirements of three times the target maneuver. (d) The magnitude of total achieved missile acceleration for the same variation of target maneuver *g* levels and for the three missile time constants considered. As the missile autopilot response time deviates further from that which PN assumes, increasingly higher acceleration levels are required from the missile.

Constant Target Acceleration Assumption

Here, all of the previous assumptions hold with the exception of target maneuver; we will assume that the target is pulling a hard-turn maneuver (i.e., constant acceleration in a particular direction). Therefore, we augment the previous (PN) state vector (where $x_1 \triangleq r_y$, $x_2 \triangleq v_y$) to include a target acceleration state $x_3 \triangleq a_{Ty}$, leading to $\bar{\mathbf{x}} \triangleq [x_1 \;\; x_2 \;\; x_3]^T$. As before, the control u is missile acceleration ($u \triangleq a_M$); the plant (process) disturbance is not considered when deriving the guidance law ($w = 0$), but it will come into play when developing a target

acceleration estimator; and the pseudo-measurement, again, is relative position ($y \triangleq x_1$). With these modeling assumptions in mind (particularly that $x_3 \triangleq a_{Ty}$ constant), the LQ optimization problem is stated as

$$\begin{aligned} \min_{u(t)} J(\bar{\mathbf{x}}(t_0), \bar{\mathbf{u}}(t_0), t_0) &= \tfrac{1}{2}\| \bar{\mathbf{x}}(t_f) \|^2_{\mathbf{Q}_f} + \tfrac{1}{2}\int_{t_0}^{t_f} u^2(t)\, dt \\ \text{Subject to: } \dot{\bar{\mathbf{x}}}(t) &= \begin{bmatrix} 0 & 1 & 0 \\ 0 & 0 & 1 \\ 0 & 0 & 0 \end{bmatrix} \bar{\mathbf{x}}(t) + \begin{bmatrix} 0 \\ -1 \\ 0 \end{bmatrix} u(t), \\ y(t) &= [1 \;\; 0 \;\; 0]\bar{\mathbf{x}}(t). \end{aligned} \tag{25}$$

As before (Eq. 20), the terminal penalty matrix is defined as $\mathbf{Q}_f = \text{diag}\{b, c, 0\}$. Following a solution procedure identical to that outlined previously, we obtain the following general solution:

$$u_2(t) = \frac{3}{t_{go}^2}\left[\frac{\left(1 + \frac{1}{2}ct_{go}\right)x_1(t) + \left(1 + \frac{1}{3}ct_{go} + \frac{c}{bt_{go}^2}\right)x_2(t)t_{go} + \frac{1}{2}\left(1 + \frac{1}{6}ct_{go} + \frac{2c}{bt_{go}^2}\right)x_3(t)t_{go}^2}{1 + \frac{3}{bt_{go}^3}(1 + ct_{go}) + \frac{ct_{go}}{4}}\right]. \tag{26}$$

If we compare the guidance law in Eq. 26 to our previous result (Eq. 21), it is clear that the only difference is in the numerator; Eq. 26 includes the addition of a (time-varying) gain multiplying the target acceleration state. Therefore, in addition to requiring estimates of relative position, relative velocity, and time-to-go, the new law also requires an estimate of target acceleration. This requirement has implications on the guidance filter structure, as we will see later. More important, estimating target acceleration given a relative position (pseudo-)measurement can be very noisy unless the measurement quality is very good. Hence, if sensor quality is not sufficient, leading to a target acceleration estimate that is too noisy, then guidance law performance could actually be worse than if we simply used PN to begin with. These factors must be carefully considered during the missile design phase.

Special Case 1: Augmented PN

If we assume that $c = 0$ and we evaluate $\lim_{b \to \infty} u_2(t) = u_{\text{APN}}(t)$, then Eq. 26 collapses to the well-known augmented PN (APN) guidance law:

$$u_{APN}(t) = \frac{3}{t_{go}^2}\left[x_1(t) + x_2(t)t_{go} + \tfrac{1}{2}x_3(t)t_{go}^2\right]. \tag{27}$$

Leveraging the discussion above, if we compare Eq. 27 to the expression for PN given in Eq. 22, the only difference is the addition of the $\frac{1}{2}a_T t_{go}^2$ term in the numerator of the APN guidance law. Thus, for APN, the effective navigation ratio is the same as in PN guidance ($\tilde{N}\big|_{APN} = 3$), but the ZEM estimate is now given by $ZEM_{APN} = r_y(t) + v_y(t)t_{go} + \frac{1}{2}a_T(t)t_{go}^2$.

Special Case 2: Augmented REN Guidance Law

If we evaluate $\lim_{b,c \to \infty} u_2(t) = u_{\text{AREN}}(t)$, then Eq. 26 collapses to the augmented REN (AREN) guidance law:

$$u_{\mathrm{AREN}}(t) = \frac{6}{t_{go}^2}\left[x_1(t) + \tfrac{2}{3}x_2(t)\,t_{go}\right] + x_3(t)\,. \quad (28)$$

Notice that, unlike the APN law given in Eq. 27, the AREN guidance law calls for a direct cancellation of the target maneuver term in the acceleration command.

Example Results: Maneuver Requirements for PN Versus APN

Here, in a similar approach to that found in Ref. 13, we compare the maneuver requirements for PN and APN guidance laws versus a target that pulls a hard-turn maneuver under ideal conditions (e.g., no sensor measurement noise or interceptor lag). Recall that the PN guidance law is derived assuming that the target does not maneuver, whereas the key APN assumption is that the target pulls a hard turn.

Assuming that the interceptor responds perfectly to PN acceleration commands, using Eq. 22 we can write the following second-order differential equation:

$$\frac{d^2}{dt^2}r_y(t) = a_T(t) - \frac{N}{(t_f - t)^2}\left[r_y(t) + v_y(t)\,(t_f - t)\right]. \quad (29)$$

Note that we have left the navigation gain as the variable N. Next, we assume zero initial conditions—$r_y(0) = 0$, $v_y(0) = 0$—and use Maple to solve Eq. 29, thus giving analytic expressions for $r_y(t)$ and $v_y(t)$. We then take $r_y(t)$ and $v_y(t)$ and reinsert them into Eq. 22 to obtain the following expression for missile acceleration caused by a hard-turn target maneuver:

$$a_{\mathrm{M}_{PN}}(t) = \frac{N}{N-2}\left[1 - \left(1 - \frac{t}{t_f}\right)^{N-2}\right]a_T\,. \quad (30)$$

For the APN case, we employ an analogous procedure, using Eq. 27 as the starting point. For this case, we obtain the following expression for missile acceleration, given that the target pulls a hard-turn maneuver:

$$a_{\mathrm{M}_{\mathrm{APN}}}(t) = \frac{N}{2}\left[1 - \frac{t}{t_f}\right]^{N-2} a_T\,. \quad (31)$$

Figure 7 illustrates a comparison of PN and APN acceleration requirements for various guidance gain values versus a target pulling a hard turn, via Eqs. 30 and 31, respectively. Referring to Fig. 7, we see that PN (solid lines) demands an increasing level of missile acceleration as flight time increases. In fact, for a guidance gain of 3, PN requires three times the acceleration of the target to effect an intercept; hence, the well-known 3-to-1 ratio rule of thumb. If we increase the guidance gain, theory says that the theoretical 3-to-1 rule of thumb can be relaxed. In practice, however, higher gains may lead to excessive noise throughput, perhaps negating any theoretically perceived benefits.

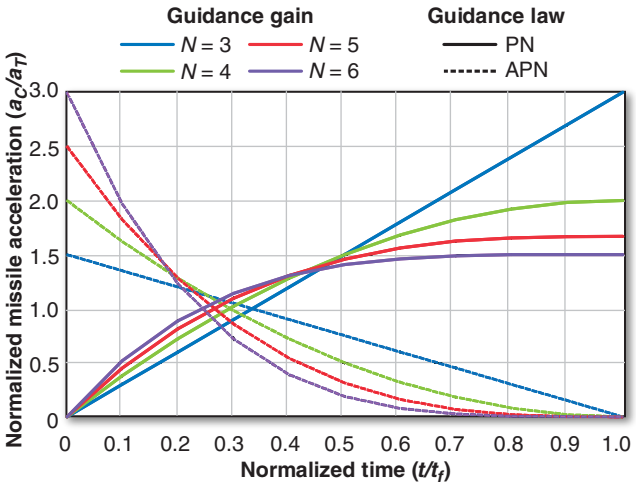

Figure 7. A comparison is made of PN and APN acceleration requirements for various guidance gain values versus a target pulling a hard turn. PN results (solid lines) indicate that PN demands an increasing level of missile acceleration as flight time increases. Notice that for a guidance gain of 3, PN requires three times the acceleration of the target to effect an intercept; hence, the well-known 3-to-1 ratio rule of thumb. Increasing the guidance gain can theoretically relax the 3-to-1 rule of thumb, but higher gains may lead to excessive noise throughput. The graph illustrates that APN (dashed lines) is more anticipatory in that it demands maximum acceleration at the beginning of the engagement and less as engagement time increases. Note that for a guidance gain of 3, APN (theoretically) requires half the acceleration that PN does when engaging a target that is pulling a hard turn.

Unlike PN, APN (dashed lines in Fig. 7) is more anticipatory in that it demands maximum acceleration at the beginning of the engagement and less acceleration as engagement time increases. Moreover, note that for a guidance gain of 3, APN (theoretically) requires half the acceleration that PN does when engaging a target that is pulling a hard turn. Note that, for a guidance gain of 4, the theoretical acceleration requirements for PN and APN are the same and, for gains above 4, APN demands more acceleration than PN (although saturating the acceleration command early is not nearly the problem that saturating late is).

Constant Target Jerk Assumption

The assumptions stated during the derivation of APN are still valid with the exception of target maneuver; here, we will assume that the target acceleration is linearly increasing (i.e.,

constant jerk in a particular direction). This may be a reasonable assumption, for example, in order to develop a terminal homing guidance strategy for use during boost-phase ballistic missile defense, where it is necessary to engage and destroy the enemy missile while it is still boosting. In such a context, it is possible that a linearly increasing acceleration model (assumption) better reflects actual target maneuver (acceleration) as compared to the APN assumption. Therefore, we augment the previous (PN) state vector (where $x_1 \triangleq r_y$, $x_2 \triangleq v_y$) to include a target acceleration state $x_3 \triangleq a_{Ty}$ and a target jerk state $x_4 \triangleq \dot{x}_3 = j_{Ty}$, leading to $\bar{\mathbf{x}} \triangleq [x_1 \;\; x_2 \;\; x_3 \;\; x_4]^T$. As before, the control u is missile acceleration ($u \triangleq a_M$), the plant (process) disturbance is not considered ($w = 0$), but it will come into play when developing a target state estimator, and the pseudo-measurement, again, is relative position ($y \triangleq x_1$). With these modeling assumptions in mind (particularly that $x_4 \triangleq j_{Ty} \equiv$ constant), the LQ optimization problem is stated as

$$\min_{u(t)} J(\bar{\mathbf{x}}(t_0), \bar{\mathbf{u}}(t_0), t_0) = \tfrac{1}{2}\| \bar{\mathbf{x}}(t_f) \|^2_{\mathbf{Q}_f} + \tfrac{1}{2}\int_{t_0}^{t_f} u^2(t)\, dt$$

$$\text{Subject to: } \dot{\bar{\mathbf{x}}}(t) = \begin{bmatrix} 0 & 1 & 0 & 0 \\ 0 & 0 & 1 & 0 \\ 0 & 0 & 0 & 1 \\ 0 & 0 & 0 & 0 \end{bmatrix} \bar{\mathbf{x}}(t) + \begin{bmatrix} 0 \\ -1 \\ 0 \\ 0 \end{bmatrix} u(t), \tag{32}$$

$$y(t) = [1 \;\; 0 \;\; 0 \;\; 0]\bar{\mathbf{x}}(t).$$

Defining the terminal penalty matrix to be $\mathbf{Q}_f = \text{diag}\{b, c, 0, 0\}$, and following a solution procedure identical to that outlined previously, we obtain the following general solution:

$$u_3(t) = \frac{3}{t_{go}^2}\left[\frac{\left(1 + \frac{ct_{go}}{2}\right)x_1(t) + \left(1 + \frac{ct_{go}}{3} + \frac{c}{bt_{go}^2}\right)x_2(t)t_{go} + \frac{1}{2}\left(1 + \frac{ct_{go}}{6} + \frac{2c}{bt_{go}^2}\right)x_3(t)t_{go}^2 + \frac{1}{6}\left(1 + \frac{3c}{bt_{go}^2}\right)x_4(t)t_{go}^3}{1 + \frac{3}{bt_{go}^3}(1 + ct_{go}) + \frac{ct_{go}}{4}}\right]. \tag{33}$$

If we compare the guidance law in Eq. 33 to our previous result (Eq. 26), we see, again, that the only difference is in the numerator; Eq. 33 includes the addition of a (time-varying) gain multiplying the target jerk state. Analogous to the previous case, this has (additional) implications on the guidance filter structure. More important, estimating target jerk given a relative position (pseudo-)measurement can be very noisy unless the measurement quality is excellent. If sensor quality is not sufficient, then guidance law performance could be significantly worse than if we simply used PN or APN to begin with.

Special Case 1: Extended PN

If we assume that $c = 0$ and we evaluate $\lim_{b\to\infty} u_3(t) = u_{EPN}(t)$, then Eq. 33 collapses to the extended PN (EPN) guidance law

$$u_{EPN}(t) = \frac{3}{t_{go}^2}\left[x_1(t) + x_2(t)t_{go} + \tfrac{1}{2}x_3(t)t_{go}^2 + \tfrac{1}{6}x_4(t)t_{go}^3\right]. \tag{34}$$

By this time, a pattern should be emerging regarding the current line of guidance laws. For example, if we compare PN (Eq. 22), APN (Eq. 27), and EPN (Eq. 34), we see that the effective navigation ratios for these three cases are all the same constant:

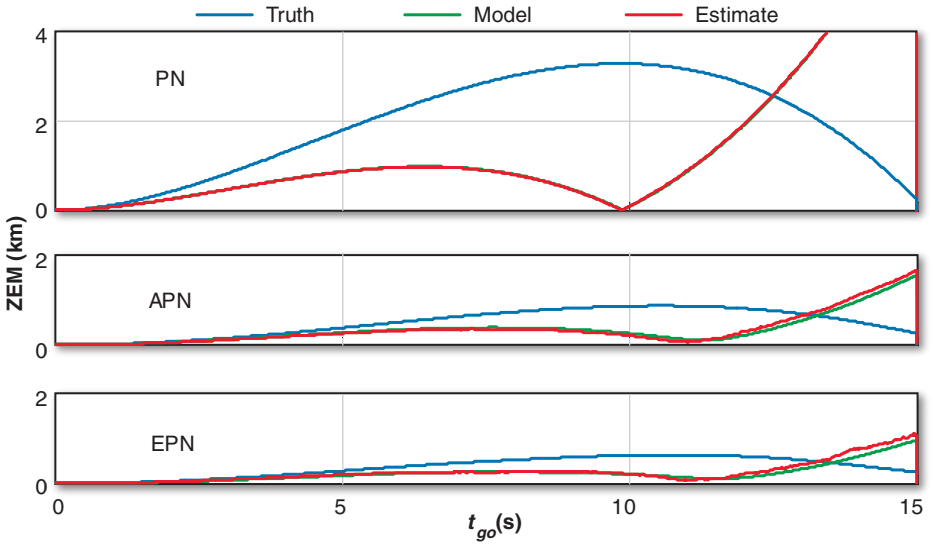

Figure 8. Comparison of ZEM removal against a boosting threat. Plots of the predicted ZEM for PN, APN, and EPN guidance laws are illustrated. Here, "truth" is computed by integrating forward a duplicate of the threat truth model and propagating the kill vehicle ballistically. The "model" curve reflects the assumed ZEM calculation for the particular guidance law, using truth data. The "estimate" curve is this same calculation with estimated data (via noisy measurements), as must be used in practice. Intercept is achieved at $t_{go} = 0$ in each case, since the ZEM goes nearly to zero. The magnitude of the ZEM is plotted; in each plot, the portion of the model-based ZEM and estimated ZEM to the right of 12 s is in the opposite direction from the true ZEM.

$$\tilde{N}\big|_{PN} = \tilde{N}\big|_{APN} = \tilde{N}\big|_{EPN} = 3\,.$$

It is the ZEM estimates that evolve from

$$ZEM_{PN} = r_y(t) + v_y(t)\,t_{go}\,, \text{ to}$$

$$ZEM_{APN} = ZEM_{PN} + \tfrac{1}{2}a_T(t)\,t_{go}^2\,, \text{ and now to}$$

$$ZEM_{EPN} = ZEM_{APN} + \tfrac{1}{6}j_T(t)\,t_{go}^3\,.$$

With regard to EPN, the addition of target acceleration and target jerk states will dictate a more complex guidance filter structure, and it may be very sensitive to sensor noise and actual target maneuver modalities as compared with PN or APN. We also note that, if we evaluate $\lim_{b,c\to\infty} u_3(t)$, then Eq. 33 collapses to the AREN guidance law previously given in Eq. 28.

A simulation study of PN, APN, and EPN guidance laws against a boosting threat illustrates the benefits of better matching the target assumptions to the intended target. In this engagement, an exoatmospheric kill vehicle intercepts a threat that accelerates (boosts) according to the ideal rocket equation, with a maximum 8.5-*g* threat acceleration occurring at intercept. Figure 8 shows how the ZEM prediction for each guidance law compares with the true ZEM as each evolves over time and under the control of the relevant guidance law. Each of the models of ZEM has significant error initially (the direction is wrong, causing the truth to increase while the assumed ZEM decreases), but for an assumed target maneuver model that more closely matches the actual target maneuver (i.e., EPN), this error is much less and the sign of the ZEM is correct sooner. The curves also show some trade-off in estimate quality (noise) as more derivatives are used in the calculation. Figure 9 demonstrates the resulting acceleration commands and fuel usage for the different guidance laws via logging of the resultant ΔV, which is defined as

$$\int_{t_0}^{t_f} |\,\bar{\mathbf{a}}_M(\tau)\,|\,d\tau\,,$$

where $\bar{\mathbf{a}}_M$ is the achieved acceleration vector. The required ΔV (translating to fuel usage) for PN, at 1356 m/s, is substantially more than APN, at 309 m/s, or EPN, at 236 m/s. The required acceleration capability of the kill vehicle also is substantially different, with PN requiring 27 *g* capability, APN requiring 3.7 *g*, and EPN requiring 3.2 *g*.

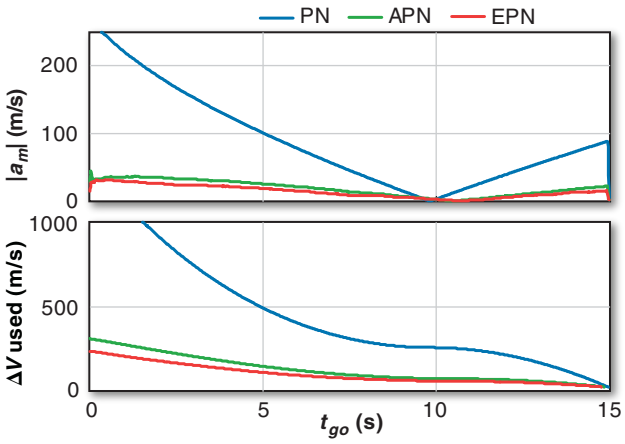

Figure 9. Acceleration command history and cumulative ΔV used for PN, APN, and EPN guidance laws versus a boosting threat. The progression is from right to left as time-to-go (t_{go}) decreases toward intercept in this single-simulation run.

Non-Ideal Missile Response Assumption

Here, the assumptions stated during the derivation of APN are still valid, save for that pertaining to a perfect missile response. Instead, we will add the more realistic assumption that the missile responds to an acceleration command via the first-order lag transfer function

$$a_M(s)/a_c(s) = \frac{1}{Ts+1},$$

hence the reference to a non-ideal missile response. The time constant, T, is a composite (roll-up) function of the missile response at a specific flight condition and depends largely on the missile aerodynamic characteristics and flight control system design. We augment the previous (APN) state vector (where $x_1 \triangleq r_y$, $x_2 \triangleq v_y$, and $x_3 \triangleq a_{Ty}$) to include a missile acceleration state $x_4 \triangleq a_{My}$, leading to $\bar{\mathbf{x}} \triangleq [x_1 \;\; x_2 \;\; x_3 \;\; x_4]^T$. (Note that the fourth state here is missile acceleration, not target jerk as was the case when deriving EPN guidance law.) As before, the control u is missile acceleration ($u \triangleq a_M$), the plant (process) disturbance is not considered ($w = 0$), but it will come into play when developing a target acceleration estimator, and the pseudo-measurement, again, is relative position ($y \triangleq x_1$). In addition, we add a missile accelerometer measurement. With these modeling assumptions in mind, the LQ optimization problem is stated as

$$\begin{aligned}
&\min_{u(t)} J(\bar{\mathbf{x}}(t_0), \bar{\mathbf{u}}(t_0), t_0) = \tfrac{1}{2}\|\bar{\mathbf{x}}(t_f)\|^2_{\mathbf{Q}_f} + \tfrac{1}{2}\int_{t_0}^{t_f} u^2(t)\,dt \\
&\text{Subject to: } \dot{\bar{\mathbf{x}}}(t) = \begin{bmatrix} 0 & 1 & 0 & 0 \\ 0 & 0 & 1 & -1 \\ 0 & 0 & 0 & 0 \\ 0 & 0 & 0 & -\frac{1}{T} \end{bmatrix} \bar{\mathbf{x}}(t) + \begin{bmatrix} 0 \\ 0 \\ 0 \\ \frac{1}{T} \end{bmatrix} u(t), \qquad (35) \\
&y(t) = \begin{bmatrix} 1 & 0 & 0 & 0 \\ 0 & 0 & 0 & 1 \end{bmatrix} \bar{\mathbf{x}}(t).
\end{aligned}$$

Here, we do not consider a terminal velocity penalty in order to reduce overall guidance law complexity, which leads to the terminal penalty matrix given by $\mathbf{Q}_f = \text{diag}\{b, 0, 0, 0\}$. Thus, following an identical solution procedure to that outlined previously, we obtain the following general guidance law solution:

$$u_4 = \frac{6\left(\frac{t_{go}}{T}\right)^2}{t_{go}^2} \frac{\left(\frac{t_{go}}{T} + e^{-t_{go}/T} - 1\right)\left[x_1(t) + x_2(t)t_{go} + \frac{1}{2}t_{go}^2 x_3(t) - T^2\left(\frac{t_{go}}{T} + e^{-t_{go}/T} - 1\right)x_4(t)\right]}{\frac{6}{bT^3} + \left(3 + 6\frac{t_{go}}{T} - 6\frac{t_{go}^2}{T^2} + 2\frac{t_{go}^3}{T^3} - 12\frac{t_{go}}{T}e^{-t_{go}/T} - 3e^{-2t_{go}/T}\right)}. \qquad (36)$$

Upon examination of Eq. 36, it becomes clear that the non-ideal missile response assumption adds additional complexity to the guidance law structure (remember that we have not considered a terminal penalty on relative velocity, i.e., $c = 0$). To better visualize this complexity, consider the constant target acceleration guidance law given in Eq. 26. If we take $\lim_{c \to 0} u_2(t)$, we obtain the following result:

$$u_2(t)\big|_{c=0} = \frac{3}{t_{go}^2}\left[\frac{x_1(t) + x_2(t)t_{go} + \frac{1}{2}x_3(t)t_{go}^2}{1 + \frac{3}{bt_{go}^3}}\right]. \qquad (37)$$

The structure of Eq. 37 is significantly less complex than that given in Eq. 36 despite the fact that the cost function for both is identical (i.e., b is finite and $c = 0$).

If we take $\lim_{b \to \infty} u_4(t)$, we obtain the well-known "optimal" guidance law (OGL) referred to in many texts (see Refs. 7, 13, and 14 for examples):

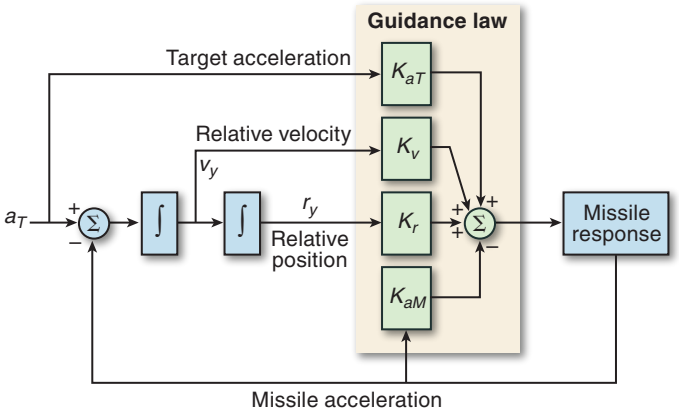

Gain	Guidance law		
	PN	APN	OGL
K_r	$\frac{3}{t_{go}^2}$	$\frac{3}{t_{go}^2}$	$\frac{\tilde{N}}{t_{go}^2}$
K_v	$\frac{3}{t_{go}}$	$\frac{3}{t_{go}}$	$\frac{\tilde{N}}{t_{go}}$
K_{aT}	0	$\frac{3}{2}$	$\frac{\tilde{N}}{2}$
K_{aM}	0	0	$\frac{-\tilde{N}T^2}{t_{go}^2}\left(\frac{t_{go}}{T}+e^{-t_{go}/T}-1\right)$
$\tilde{N}\|_{OGL} \triangleq \frac{6\left(\frac{t_{go}}{T}\right)^2\left(\frac{t_{go}}{T}+e^{-t_{go}/T}-1\right)}{\left(3+6\frac{t_{go}}{T}-6\frac{t_{go}^2}{T^2}+2\frac{t_{go}^3}{T^3}-12\frac{t_{go}}{T}e^{-t_{go}/T}-3e^{-2t_{go}/T}\right)}$			

Figure 10. The feedback structure of the PN, APN, and OGL guidance laws is depicted here. The relative complexity of the different guidance laws is established as we add additional assumptions regarding the engagement and missile response characteristics. The diagram emphasizes the fact that a substantial increase in complexity arises when the assumptions move from an ideal to non-ideal interceptor response assumption.

$$u_{OGL} = \frac{6\left(\frac{t_{go}}{T}\right)^2}{t_{go}^2}\frac{\left(\frac{t_{go}}{T}+e^{-t_{go}/T}-1\right)\left[x_1(t)+x_2(t)t_{go}+\frac{1}{2}t_{go}^2x_3(t)-T^2\left(\frac{t_{go}}{T}+e^{-t_{go}/T}-1\right)x_4(t)\right]}{\left(3+6\frac{t_{go}}{T}-6\frac{t_{go}^2}{T^2}+2\frac{t_{go}^3}{T^3}-12\frac{t_{go}}{T}e^{-t_{go}/T}-3e^{-2t_{go}/T}\right)}. \quad (38)$$

Referring back to the APN law presented in Eq. 27, a couple of important points are noted. First, we compare the APN ZEM estimate given by

$$ZEM_{APN} = x_1(t) + x_2(t)t_{go} + \frac{1}{2}t_{go}^2x_3(t)$$

with that in Eq. 38 and see that the OGL ZEM estimate is

$$ZEM_{OGL} = ZEM_{APN} - T^2\left(\frac{t_{go}}{T}+e^{-t_{go}/T}-1\right)x_4(t).$$

In addition, the effective navigation ratio for APN is given by $\tilde{N}|_{APN} = 3$. In contrast, from Eq. 38, $\tilde{N}|_{OGL}$ is time-varying and can be expressed as shown below:

$$\tilde{N}|_{OGL} \triangleq \frac{6\left(\frac{t_{go}}{T}\right)^2\left(\frac{t_{go}}{T}+e^{-t_{go}/T}-1\right)}{\left(3+6\frac{t_{go}}{T}-6\frac{t_{go}^2}{T^2}+2\frac{t_{go}^3}{T^3}-12\frac{t_{go}}{T}e^{-t_{go}/T}-3e^{-2t_{go}/T}\right)}. \quad (39)$$

For illustrative purposes, Fig. 10 depicts the feedback structure of the PN, APN, and OGL guidance laws discussed this far and thus helps to establish the relative complexity of the different guidance laws as we add additional assumptions regarding the engagement and missile response. From Fig. 10, it is obvious that a substantial increase in complexity arises when the assumptions move from an ideal to non-ideal interceptor response assumption.

Example Comparisons of PN, APN, and OGL

In this example, Fig. 11 illustrates the miss distance and called-for acceleration statistics for PN, APN, and OGL guidance laws versus a target pulling a 5-*g* hard turn. The Monte Carlo data are displayed in cumulative probability form. From Fig. 11, we

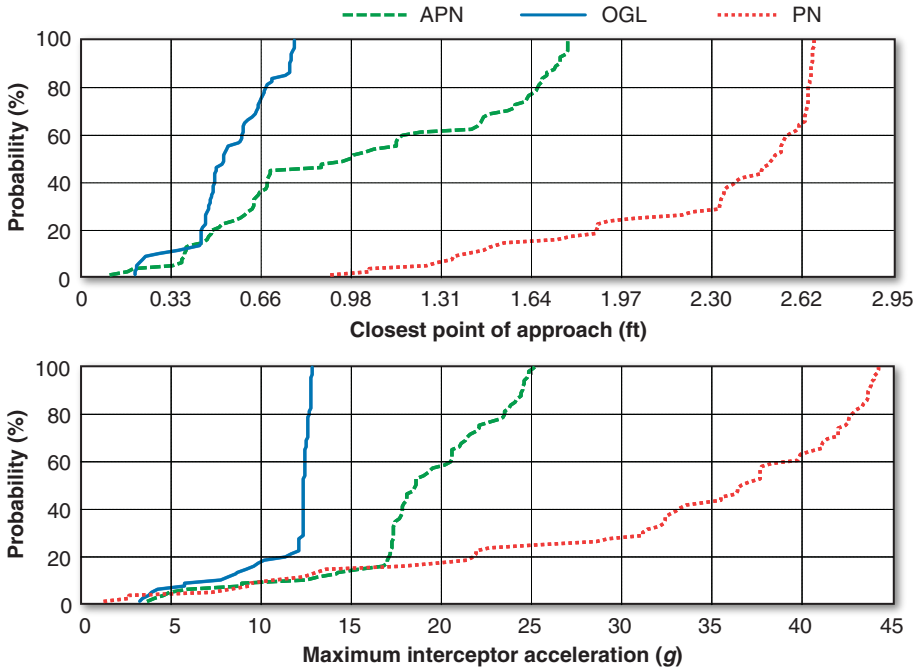

Figure 11. The cumulative probability performance of PN, APN, and OGL guidance laws versus a 5-*g* hard-turn target is shown. Both the cumulative probability of the maximum interceptor acceleration and CPA for 100-run Monte Carlo sets are plotted. With these graphs, it is easy to quickly ascertain the probability of achieving the *x*-axis parameter value (e.g., maximum acceleration). In both graphs, lines that are more vertical and farther to the left are considered more desirable. All noise and error sources are turned off, but the target maneuver start time is randomized over the last second of terminal homing. Note that the actual missile response model is non-ideal, and it varies with the flight conditions of the missile trajectory.

see a distinct trend considering PN versus APN versus OGL guidance laws. Given that PN is derived assuming the target is not maneuvering, we expect the performance to degrade if the target does maneuver. It also is not surprising to see that, statistically, more acceleration is required versus APN or OGL. The improvement from APN to OGL is explained by the fact that APN assumes a perfect missile response to acceleration commands and OGL assumes that the missile responds as a first-order lag (refer back to Eq. 27 compared with Eq. 38).

TIME-TO-GO ESTIMATION

As shown in the previous section, *Extensions to PN: Other Optimal Homing Guidance Laws*, many modern guidance laws require an estimate of time-to-go (t_{go}), which is the time it will take the missile to intercept the target or to arrive at the closest point of approach (CPA). The t_{go} estimate also is a critical quantity for missiles that carry a warhead that must detonate when the missile is close to the target. For example, recall the general optimal guidance law shown in Eq. 36. This guidance law can be expressed as $\tilde{N} \times ZEM$, where

$$ZEM = \left[x_1(t) + x_2(t)t_{go} + \tfrac{1}{2}t_{go}^2 x_3(t) - T^2\left(\tfrac{t_{go}}{T} + e^{-t_{go}/T} - 1\right)x_4(t)\right]$$

and the effective navigation ratio, $\tilde{N}$, is shown in Eq. 40, where b and T represent the terminal miss penalty and assumed missile time constant, respectively (see the section *Non-Ideal Missile Response Assumption*, wherein Eq. 36 was derived, for a further description):

$$\tilde{N} = \frac{6\left(\frac{t_{go}}{T}\right)^2\left(\frac{t_{go}}{T} + e^{-t_{go}/T} - 1\right)}{\frac{6}{bT^3} + \left(3 + 6\frac{t_{go}}{T} - 6\frac{t_{go}^2}{T^2} + 2\frac{t_{go}^3}{T^3} - 12\frac{t_{go}}{T}e^{-t_{go}/T} - 3e^{-2t_{go}/T}\right)}. \quad (40)$$

It is clear from Eq. 40 that $\tilde{N}$ is a function of t_{go}. Figure 12 illustrates the t_{go} dependence of the general optimal guidance law effective navigation ratio for three values of terminal miss penalty. The curves are normalized with respect to the missile time constant T. Referring to Fig. 12, consider the b = 1000 curve. As $t_{go}/T \to 2$, $\tilde{N}$ achieves its maximum value and then reduces as $t_{go}/T \to 0$. Clearly, this guidance law gain curve evolves in a way that places much greater emphasis on ZEM at certain times near intercept. Imagine that the actual (true) t_{go} is 2 s but that the estimate of t_{go} is in error and biased toward the positive direction by four missile time constants ($4T$). Then, from Fig. 12 we can see that the guidance gain would be about one-seventh of what it should be at $t_{go}/T = 2$, thereby not placing optimal emphasis on ZEM at that time, and degrading overall guidance performance.

The simplest time-to-go estimation scheme uses measurements (or estimates) of range and range rate. Consider the engagement geometry of Fig. 13, where $\bar{\mathbf{v}}_M$ = missile velocity, $\bar{\mathbf{v}}_T$ = target velocity, $\bar{\mathbf{r}}$ = target–missile relative

$$\tilde{N} \triangleq \frac{\frac{6}{T^2}\left(\frac{t_{go}}{T} + e^{-t_{go}/T} - 1\right)}{\frac{6}{bT^3} + \left(3 + 6\frac{t_{go}}{T} - 6\frac{t_{go}^2}{T^2} + 2\frac{t_{go}^3}{T^3} - 12\frac{t_{go}}{T}e^{-t_{go}/T} - 3e^{-2t_{go}/T}\right)}$$

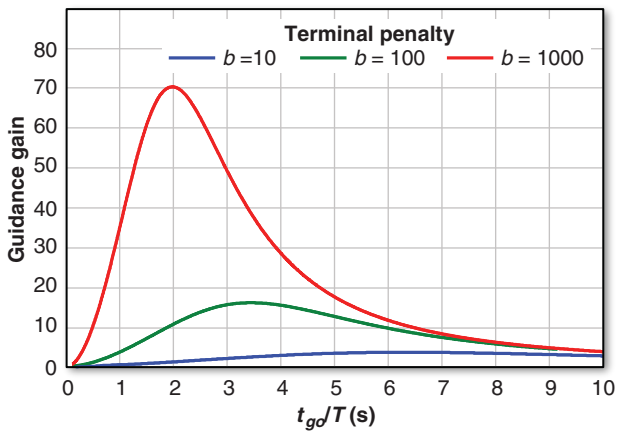

Figure 12. The normalized t_{go} dependence of the effective navigation ratio $\tilde{N}$ for the OGL is shown here for three terminal penalty values. Normalization is with respect to the missile time constant T. We note that, as t_{go} approaches infinity, the effective navigation ratio always approaches 3.

position, and $\bar{\mathbf{v}}$ = target–missile relative velocity. Referring to Fig. 13, we assume that the missile can measure or estimate relative range ($R = \|\bar{\mathbf{r}}\|$) to the target and range rate ($\dot{R}$) along the LOS to the target. If we assume that the missile and target speeds are constant, then one can estimate time-to-go as

$$\hat{t}_{go} = -\frac{R}{\dot{R}}. \tag{41}$$

Another common approach to estimating time-to-go also assumes that the missile and target speeds are constant. Define $\Delta t \triangleq t^* - t$, where t is the current time and t^* is a future time. Thus, given estimates of target–missile relative position and relative velocity at the current time t, the future target–missile relative position at time t^* is given as

$$\bar{\mathbf{r}}(t^*) = \bar{\mathbf{r}}(t) + \bar{\mathbf{v}}(t)\Delta t. \tag{42}$$

At the CPA, the following condition holds:

$$\bar{\mathbf{r}}(t^*) \cdot \bar{\mathbf{v}}(t^*) = 0. \tag{43}$$

This condition is illustrated in Fig. 13 by the perpendicular line from the target to the relative velocity. Based on our assumptions, using Eq. 42 in Eq. 43, and recognizing the constant velocity assumption, we obtain the following expression for $\Delta t \equiv t_{go}$:

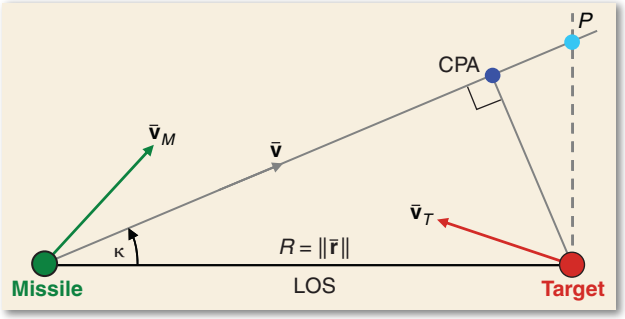

Figure 13. The missile–target (planar) engagement geometry is shown here. This depiction places the LOS to the target along the x axis of the coordinate system. Missile and target velocity vectors are indicated as $\bar{\mathbf{v}}_M$ and $\bar{\mathbf{v}}_T$, respectively. The relative velocity, $\bar{\mathbf{v}}$, makes an angle κ with the LOS and passes through the points indicated by CPA and P.

$$t_{go} = -\frac{\bar{\mathbf{r}}(t) \cdot \bar{\mathbf{v}}(t)}{\bar{\mathbf{v}}(t) \cdot \bar{\mathbf{v}}(t)}. \tag{44}$$

Using this expression for t_{go} in Eq. 42, we obtain the target–missile relative separation at the CPA:

$$\begin{aligned} \bar{\mathbf{r}}_{\mathrm{CPA}} &= \frac{\bar{\mathbf{r}}(t)[\bar{\mathbf{v}}(t) \cdot \bar{\mathbf{v}}(t)] - \bar{\mathbf{v}}(t)[\bar{\mathbf{r}}(t)(t) \cdot \bar{\mathbf{v}}(t)]}{\bar{\mathbf{v}}(t) \cdot \bar{\mathbf{v}}(t)} \\ &= \frac{[\bar{\mathbf{v}}(t) \times \bar{\mathbf{r}}(t)] \times \bar{\mathbf{v}}(t)}{\bar{\mathbf{v}}(t) \cdot \bar{\mathbf{v}}(t)}. \end{aligned} \tag{45}$$

Conceptually, the differences between time-to-go estimation using Eq. 41 rather than Eq. 44 can be explained by using Fig. 13. For this discussion, and without loss of generality, we assume that the missile velocity is constant and that the target is stationary. Referring to Fig. 13, we see that Eq. 41 estimates the flight time for the missile to reach point P. However, Eq. 44 estimates the time it takes for the missile to reach the CPA. If the missile and target have no acceleration (the up-front assumption during the derivation), then Eq. 44 is exact.

CLOSING REMARKS

In this article, we have focused on developing homing guidance laws by using optimal control techniques. To this end, a number of modern guidance laws (PN and beyond) were derived using LQ optimal control methods. We note that, regardless of the specific structure of the guidance law (e.g., PN versus OGL), we developed the relevant guidance law assuming that all of the states necessary to mechanize the implementation were (directly) available for feedback and uncorrupted by noise (recall we referred to this as the "perfect state information problem"). In a companion article in

this issue, "Guidance Filter Fundamentals," we point to the separation theorem, which states that the optimal solution to this problem separates into the optimal deterministic controller (i.e., the "perfect state information solution") driven by the output of an optimal state estimator. Thus, in that article, we discuss guidance filtering, which is the process of taking raw (targeting, inertial, and possibly other) sensor data as inputs and estimating the relevant signals (estimates of relative position, relative velocity, target acceleration, etc.) upon which the guidance law operates.

REFERENCES

[1]Bryson, A. E., and Ho, Y.-C., *Applied Optimal Control*, Hemisphere Publishing Corp., Washington, DC (1975).

[2]Cottrell, R. G., "Optimal Intercept Guidance for Short-Range Tactical Missiles," *AIAA J.* **9**(7), 1414–1415 (1971).

[3]Ho, Y. C., Bryson, A. E., and Baron, S., "Differential Games and Optimal Pursuit-Evasion Strategies," *IEEE Trans. Automatic Control* **AC-10**(4), 385–389 (1965).

[4]Athans, M., and Falb, P. L., *Optimal Control: An Introduction to the Theory and Its Applications*, McGraw-Hill, New York (1966).

[5]Jackson, P. B., *TOMAHAWK 1090 Autopilot Improvements: Pitch-Yaw-Roll Autopilot Design*, Technical Memorandum F1E(90)U-1-305, JHU/APL, Laurel, MD (1 Aug 1990).

[6] Basar, T., and Bernhard, P., *H-Infinity Optimal Control and Related Minimax Design Problems*, Birkhäuser, Boston (1995).

[7]Ben-Asher, J. Z., and Yaesh, I., *Advances in Missile Guidance Theory*, American Institute of Aeronautics and Astronautics, Reston, VA (1998).

[8]Grewal, M. S., and Andrews, A. P., *Kalman Filtering Theory and Practice*, Prentice Hall, Englewood Cliffs, NJ (1993).

[9]Pearson, J. D., "Approximation Methods in Optimal Control," *J. Electron. Control* **13**, 453–469 (1962).

[10]Vaughan, D. R., "A Negative Exponential Solution for the Matrix Riccati Equation," *IEEE Trans. Autom. Control* **14**(2), 72–75 (Feb 1969).

[11]Vaughan, D. R., "A Nonrecursive Algebraic Solution for the Discrete Riccati Equation," *IEEE Trans. Autom. Control* **15**(10), 597–599 (Oct 1970).

[12]Pue, A. J., *Proportional Navigation and an Optimal-Aim Guidance Technique*, Technical Memorandum F1C (2)-80-U-024, JHU/APL, Laurel, MD (7 May 1980).

[13]Zames, G., "Feedback and Optimal Sensitivity: Model Reference Transformations, Multiplicative Seminorms, and Approximate Inverses," *IEEE Trans. Autom. Control* **26**, 301–320 (1981).

[14]Shneydor, N. A., *Missile Guidance and Pursuit: Kinematics, Dynamics and Control*, Horwood Publishing, Chichester, England (1998).

The Authors

Neil F. Palumbo is a member of APL's Principal Professional Staff and is the Group Supervisor of the Guidance, Navigation, and Control Group within the Air and Missile Defense Department (AMDD). He joined APL in 1993 after having received a Ph.D. in electrical engineering from Temple University that same year. His interests include control and estimation theory, fault-tolerant restructurable control systems, and neuro-fuzzy inference systems. Dr. Palumbo also is a lecturer for the JHU Whiting School's Engineering for Professionals program. He is a member of the Institute of Electrical and Electronics Engineers and the American Institute of Aeronautics and Astronautics. **Ross A. Blauwkamp** received a B.S.E. degree from Calvin College in 1991 and an M.S.E. degree from the University of Illinois in 1996; both degrees are in electrical engineering. He is pursuing a Ph.D. from the University of Illinois. Mr. Blauwkamp joined APL in May 2000 and currently is the supervisor of the Advanced Concepts and Simulation Techniques Section in the Guidance, Navigation, and Control Group of AMDD. His interests include dynamic games, nonlinear control, and numerical methods for control. He is a member of the Institute of Electrical and Electronics Engineers and the American Institute of Aeronautics and Astronautics. **Justin M. Lloyd** is a member of the APL Senior Professional Staff in the Guidance, Navigation, and Control Group of AMDD. He holds a B.S. in mechanical engineering from North Carolina State University and an M.S. in mechanical engineering from Virginia Polytechnic Institute and State University. Currently, Mr. Lloyd is pursuing his Ph.D. in electrical engineering at The Johns Hopkins University. He joined APL in 2004 and conducts work in optimization; advanced missile guidance, navigation, and control; and integrated controller design. For further information on the work reported here, contact Neil Palumbo. His email address is neil.palumbo@jhuapl.edu.

Neil F. Palumbo

Ross A. Blauwkamp

Justin M. Lloyd

The *Johns Hopkins APL Technical Digest* can be accessed electronically at **www.jhuapl.edu/techdigest**.